

Towards roughness-based drag reduction in cross-flow dominated flows

S.J. Garrett^{1*}, A.J. Cooper^{1,2}, M. Özkan², P.J. Thomas²



Abstract

Recent theoretical results are presented from our ongoing study investigating the distinct convective instability properties of the boundary-layer flow over rough rotating disks. In this study, radial anisotropic surface roughness (concentric grooves) is modelled using the partial-slip approach of Miklavčič & Wang (2004) and the surface-geometry approach of Yoon *et al.* (2007). An energy analysis reveals that for both instability modes, the main contributors to the energy balance are the energy production by the Reynolds stresses and conventional viscous dissipation. For the Type I mode, energy dissipation increases and the Reynolds-stress energy production decreases with roughness under both models. This suggests a clear stabilising effect of the anisotropic roughness on the Type I mode. For the Type II mode, the Reynolds-stress energy production increases with roughness under both models. However, the energy dissipation of the Type II mode decreases with the roughness under the surface-geometry model and increases under the partial-slip model. This sensitivity to the precise form of the anisotropic roughness suggests that maximising dissipation by an appropriately designed roughness can theoretically lead to an overall beneficial stabilisation of both the Type I and Type II modes. This is a potential route to overall boundary-layer-transition delay and drag reduction in cross-flow dominated flows.

Keywords

Rotating boundary layers – Surface Roughness

¹Department of Engineering, University of Leicester, UK

²School of Engineering, University of Warwick, UK

*Corresponding author: stephen.garrett@le.ac.uk

1. INTRODUCTION

The von Kármán boundary layer represents a typical, generic example of a general class of fully three-dimensional boundary layers that share the common, characteristic feature of a cross-flow velocity component [1–3]. Similar boundary layers are encountered in many applied contexts such as, for instance, on the blades of wind turbines or over the highly swept wings of aircraft.

Here we study effects of distributed surface roughness on the laminar-turbulent transition process of the von Kármán boundary-layer flow. All boundary layers with a cross-flow component display similar laminar-turbulent transition characteristics due to the existence of an inflection point on the cross-flow velocity profile [2, 3]. Hence, the results presented here are of general, direct practical relevance to all applied flow configurations where a boundary layer with a cross-flow component is established. Our motivating, long-term aim is to develop theoretical methods to enable the energetically-optimal design of surface-roughness that can be exploited, for boundary layers with a cross-flow component, in the context of the development of new, passive drag-reduction techniques.

It has now been firmly established that, contrary to the classic belief, the interaction of boundary-layer flow with the *right sort of roughness* on surfaces can result in energetically beneficial, drag-reducing effects [4–6]. The challenge that remains, however, is to identify what represents the *right sort of roughness* that leads to such drag-reducing effects in any particular application. One fundamental, general strategy known to result in reduced drag is to control the laminar flow

and delay its transition to turbulence. This method of the stabilisation of the boundary-layer flow exploits the fact that laminar flows are subject to smaller dissipative energy losses than turbulent flows. The theoretical results to be discussed here will reveal clear evidence of stabilising effects of the investigated surface structures on von Kármán boundary-layers on rotating disks.

Two distinct models for the steady boundary-layer flow over rough rotating disks exist in the literature. They were developed by Yoon *et al.* [7] and Miklavčič & Wang [8] and are henceforth referred to as the YHP and MW models, respectively. Both models show how successively increasing roughness levels lead to deviations from the classic similarity solution for the flow over a smooth disk due to von Kármán [1]. The main goal of this continuing study is to demonstrate that theoretical predictions for the stability characteristics of the von Kármán boundary layer, based on the two fundamentally different modelling approaches, lead to overall consistent, and energetically beneficial, results.

The YHP approach models roughness by imposing a particular surface distribution as a function of radial position and assumes a rotational symmetry. The YHP approach therefore models roughness in the radial direction only, i.e. the flow over disks with concentric grooves of a particular cross-sectional shape profile. Alternatively, rather than imposing a particular mathematical form of the surface roughness, the MW approach models roughness empirically by replacing the usual no-slip boundary conditions with partial-slip conditions at the disk surface. The MW model is therefore capable of

modelling independent levels of roughness in the radial and azimuthal directions by separately modifying the boundary conditions in these directions.

The case of uniform levels of roughness in every direction over a surface is typically referred to as *isotropic* roughness, and non-uniform levels of roughness as *anisotropic* roughness. The MW model is clearly capable of modelling both anisotropic and isotropic roughness; the YHP model, however, is only capable of modelling the roughness in the radial direction, i.e. a particular case of anisotropic roughness.

It is important to note that the analytical results of the YHP and MW models have not yet been corroborated by experiment and so the two models should be considered as competing models of an actual flow. For this reason, it is instructive to consider a comparative study of the stability characteristics of the steady flows arising from both models. Comparisons will be made as appropriate between the stability characteristics of the YHP flows and those of ‘equivalent’ levels of radial anisotropic roughness under the MW flow.

In our previous publication [9] we have considered all classes of flows arising from the full MW model. In particular, our previous study considered isotropic roughness and two forms of anisotropic roughness: concentric grooves (radial anisotropic, as will be considered here) and radial grooves (azimuthal anisotropic). The results obtained reveal that both anisotropic and isotropic roughness results in a *stabilisation* of the Type I instability mode. In addition, in the case of radial anisotropic roughness, a significant *destabilisation* of the Type II mode is found. The emergence of the Type II mode with increasing roughness should therefore be understood as halting the beneficial roughness effects on the Type I mode. The interested reader is also referred to that paper for an extensive literature review of previous rotating-disk and surface-roughness studies.

This current paper should be considered a summary of our other paper [10] and full details can, of course, be found there.

2. THE STEADY FLOWS

2.1 The surface-geometry model due to YHP [7]

Full details of this formulation can be found in papers [7, 10]. Here it is sufficient to understand that, under the YHP approach, the lower surface is described by a particular functional form expressed within the dimensional cylindrical polar coordinate system (r^*, θ, z^*) . The disk is considered to be rotating about its axis of symmetry at a constant rotation rate Ω^* and we formulate the analysis in the rotating frame. All dimensional quantities are scaled on a characteristic length-scale given by the boundary-layer thickness, $d^* = \sqrt{\nu^*/\Omega^*}$, where ν^* is the kinematic viscosity, and a velocity scale given by $r^*\Omega^*$. This leads to the Reynolds number $Re = r^*\Omega^*d^*/\nu^* = r$.

The particular surface function used here scales to

$$s(r) = \delta \cos\left(\frac{2\pi r}{\gamma}\right) \quad (1)$$

which gives two non-dimensional control parameters: δ , the height of the roughness, and γ , the pitch of the roughness. It is useful to define the aspect ratio $a = \delta/\gamma$ which we henceforth refer to as the *roughness parameter* within the YHP model.

It is necessary to transform out the surface distribution before attempting to solve the governing equations. To this end we use a new coordinate system, (r, θ, ζ) , a modified form of the non-dimensional cylindrical polar co-ordinates, defined by the transformation $\zeta = z - s(r)$. These lead to transformed, rotationally symmetric flow components $U(r, \zeta)$, $V(r, \zeta)$ and $W(r, \zeta)$ in the radial, azimuthal and normal directions, respectively. The governing boundary-layer equations for the steady flow are then obtained after introducing variables closely related to the von Kármán similarity variables,

$$\begin{aligned} f(r, \zeta) &= \frac{1}{r}U(r, \zeta), \\ g(r, \zeta) &= \frac{1}{r}V(r, \zeta), \\ h(r, \zeta) &= W(r, \zeta) \end{aligned} \quad (2)$$

and given by

$$2f + r\frac{\partial f}{\partial r} + \frac{\partial h}{\partial \zeta} = 0, \quad (3)$$

$$rf\frac{\partial f}{\partial r} + h\frac{\partial f}{\partial \zeta} + \left(1 + r\frac{s's''}{1+s'^2}\right)f^2 = \quad (4)$$

$$(1 + s'^2)\frac{\partial^2 f}{\partial \zeta^2} + \frac{(1+g)^2}{1+s'^2}, \quad (5)$$

$$rf\frac{\partial g}{\partial r} + h\frac{\partial g}{\partial \zeta} = (1 + s'^2)\frac{\partial^2 g}{\partial \zeta^2} - 2f(1+g), \quad (6)$$

These PDEs are subject to the usual no-slip and quiescent boundary conditions in the rotating frame and can be solved using the commercially available NAG routine D03PEF.

The transformed flow field across (r, ζ) is found to vary at two distinct spatial scales in the radial direction. At the scale characterised by γ , we have a response dependent on where r is within the oscillatory cycle of the surface function (1). In addition to this oscillatory behaviour, we see a similarity-type solution scaling with r (as per von Kármán) at the larger spatial scale. For $\gamma < O(10^{-1})$, as is envisaged here, we argue that the small-scale response of the viscous flow will not occur in practice and it is a reasonable approximation to take an ensemble average of the flow field over any complete cycle in r . This approach leaves only the similarity-solution variation within the averaged flow field, $(\bar{f}(\zeta), \bar{g}(\zeta), \bar{h}(\zeta))$. Note that overbars have been introduced to denote averaged quantities. The ensemble average acts to ‘average away’ the oscillatory surface distribution, that is $s(r) = 0$ and so $\zeta \rightarrow z$. Under our approach the surface roughness is therefore seen to lead to a *modified von Kármán* flow, denoted $(\bar{f}(z), \bar{g}(z), \bar{h}(z))$.

Note that throughout this study we compute all ensemble averaged quantities at 100 regularly spaced locations over one wavelength and the results have been confirmed to be independent of the starting radial position. Our results also show that

the aspect ratio $a = \delta/\gamma$ determines the flow response and so, despite having two control parameters, we can work in terms of the single roughness parameter, a .

2.2 The partial-slip model due to MW [8]

Rather than imposing a particular mathematical form for the surface roughness, the MW approach assumes that roughness can be modelled by a modification of the no-slip conditions at the disk surface. In particular, the model assumes *partial slip* at the disk surface but is otherwise identical to the von Kármán formulation [1]; full details can be found elsewhere [8, 9]. The full MW model has two parameters η and λ (giving empirical measures of the roughness in the radial and azimuthal directions, respectively). These appear in the surface boundary conditions of the von Kármán ODEs such that

$$\begin{aligned}\bar{f}'(0) &= \lambda \bar{f}'(0), \\ \bar{g}(0) &= \eta \bar{g}'(0),\end{aligned}$$

where a prime denotes differentiation with respect to the normal spatial variable. Here we are concerned with the particular case of radial anisotropic roughnesses, consistent with the capabilities of the YHP model, and so set $\lambda = 0$.

2.3 Comparison of steady flows

Despite both models predicting a reduced radial jet and a thickened boundary layer, the areas enclosed by the radial profiles are found to increase with roughness under the YHP model and decrease in the MW model. This area is a measure of the volume of fluid transported outwards in the radial direction and accounts for the different behaviour of the axial entrainment between the two models. Given the different physical predictions arising from the two models and the empirical definition of roughness in the MW model, a direct quantitative comparison between ‘equivalent’ levels of roughness is not possible. Instead we proceed with a *qualitative* comparison of the effects of increasing roughness under both models. The particular values of η used here are therefore reasonably arbitrary and we have opted to use the maximum value of the radial jet as a matching parameter. That is, for each value of a in the YHP model, the value of η in the MW model is chosen such that the maximum values of the radial wall jet, $\max(\bar{f})$, agree. Note that the azimuthal and wall-normal components can never be matched between the two models and we emphasise again that direct quantitative comparisons should not be made.

The paired parameter values are found to be $a = 0.1 \sim \eta = 0.14$, $a = 0.2 \sim \eta = 0.57$ and $a = 0.3 \sim \eta = 1.18$ and comparisons between the resulting flow profiles can be seen in Figures 1(a), 2(a) and 3(a). We observe good agreement between the two models for small values of the roughness and an increasing discrepancy as the roughness increases.

3. CONVECTIVE INSTABILITY ANALYSIS

The two approaches used to calculate the steady flows have both resulted in similarity solutions in the scaled physical

space (r, θ, z) . The resulting flows are therefore related to the von Kármán flow, and, importantly, the stability analyses of the rotating-disk flow presented elsewhere [12, 15] are directly applicable in this current study. Full details of the governing perturbation equations can be found in those references. Here it is sufficient to understand that we conduct a normal-mode analysis with perturbations of the form

$$(\hat{u}, \hat{v}, \hat{w}, \hat{p}) = (u(z), v(z), w(z), p(z))e^{i(\alpha r + \beta Re\theta - \omega t)}.$$

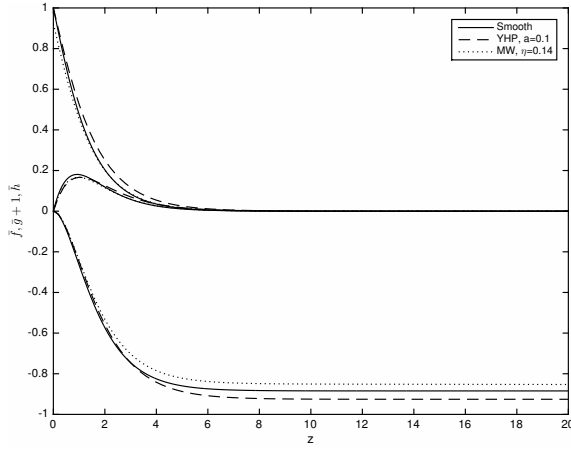
The wavenumber in the radial direction, $\alpha = \alpha_r + i\alpha_i$, is complex, as required by the spatial convective analysis to be conducted; the frequency, ω , and circumferential wavenumber, β , are real. It is assumed that β is $O(1)$ and the integer number of complete cycles of the disturbance around the azimuth is $n = \beta Re$. We identify n with the number of spiral vortices around the disk surface. Furthermore, the orientation angle of the vortices with respect to a circle centred on the axis of rotation is $\epsilon = \arctan(\beta/\alpha)$. The quantities n and ϵ can be compared directly to experimental observations. In what follows we are concerned with stationary vortices that rotate with the rough surface and so set $\omega = 0$.

The governing perturbation equations are solved using a Chebyshev polynomial discretisation method in the wall-normal direction to obtain solutions of the dispersion relation $D(\alpha, \beta; Re, [a, \eta]) = 0$ with the aim of studying the occurrence of convective instabilities for various values of the roughness parameters. The results of our code in the smooth case ($a = 0 = \eta$) have been compared against those in the literature and the predictions for the critical parameters of the Type I mode are found to be entirely consistent with other published results [11, 16–19].

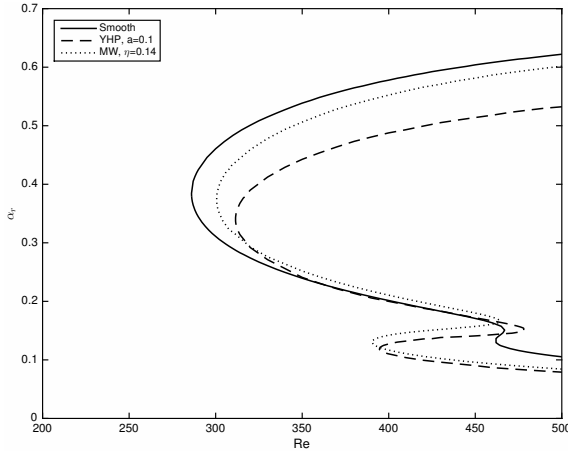
As with existing analyses of smooth rotating disks, modes of Type I and II are found to determine the convective instability properties of the disturbance modes over rough rotating disks. The Type I mode, appearing as the upper lobe in $Re - \alpha_r$ neutral curves, is known to arise from the inflectional nature of the steady-flow profiles, and the Type II mode, appearing as the lower lobe, is known to arise from streamline curvature and Coriolis effects. The neutral curves arising from the analysis of both models at comparable roughness parameters are shown in Figures 1(b), 2(b) and 3(b). The neutral curves display the same qualitative behaviour: the Type I lobe is diminished (both in terms of critical Re and width) with increased roughness, and the Type II mode exaggerated. This is entirely consistent with the results of our previous study of radial anisotropic roughness [9]. The results of the YHP model appear much more sensitive to increased roughness, although this conclusion depends somewhat on the equivalence of the parameter values used for the comparisons. Critical parameters at the onset of unstable Type I and Type II modes are given in Table 1.

4. ENERGY ANALYSIS

Following previous work [9, 10, 16] an integral energy equation for three-dimensional disturbances $(\hat{u}, \hat{v}, \hat{w})$ to the undisturbed three-dimensional boundary-layer flow (U, V, W) is



(a) Flow comparison



(b) Neutral curve comparison

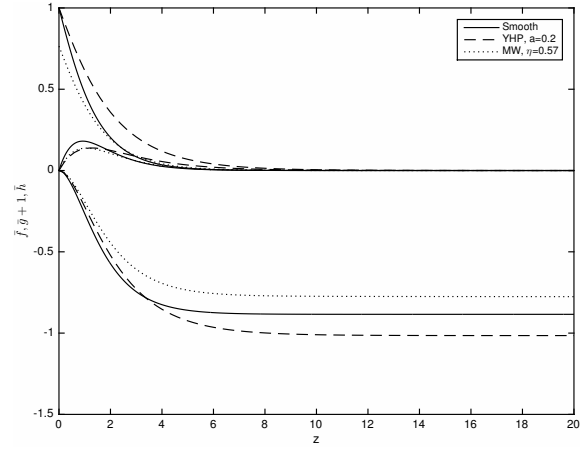
Figure 1. Model comparison at $a = 0.1$ and $\eta = 0.14$.

derived in order to extract possible underlying physical mechanisms behind the effects of roughness on the stability of rotating disk boundary-layer flow. Essentially, the energy-balance approach enables one to assess the relative influences of the various energy transfer mechanisms affecting the destabilisation of fluid disturbances. The method was used extensively for the full MW model in our previous publication [9] and full details are presented there. As demonstrated elsewhere [9, 16], the energy equation that applies to a particular eigenmode is given by

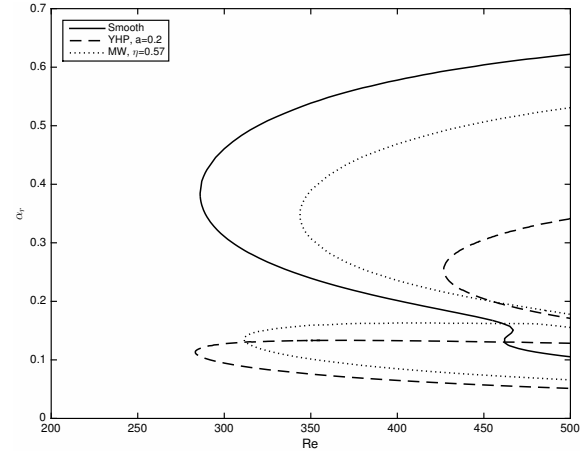
$$-2\alpha_i = \underbrace{(P_1 + P_2 + P_3)}_{\text{I}} + \underbrace{D}_{\text{II}} + \underbrace{(PW_1 + PW_2)}_{\text{III}} + \underbrace{(S_1 + S_2 + S_3)}_{\text{IV}} + \underbrace{(G_1 + G_2 + G_3)}_{\text{V}}, \quad (7)$$

where, physically, the terms on the right-hand side are identified as follows:

- (I) the Reynolds stress energy production term, obtained from $\{P_i\}$,
- (II) the viscous dissipation energy removal term, obtained



(a) Flow comparison



(b) Neutral curve comparison

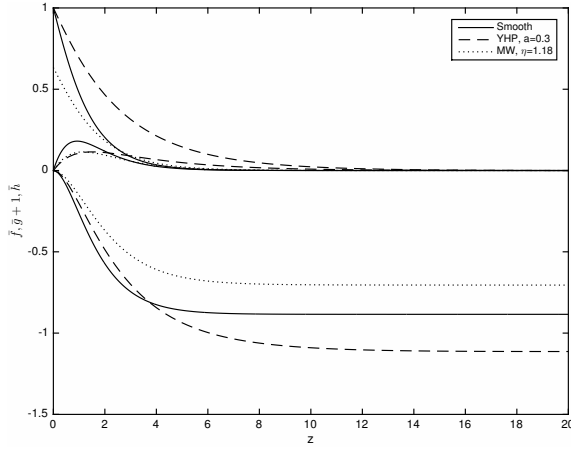
Figure 2. Model comparison at $a = 0.2$ and $\eta = 0.57$.

from D ,

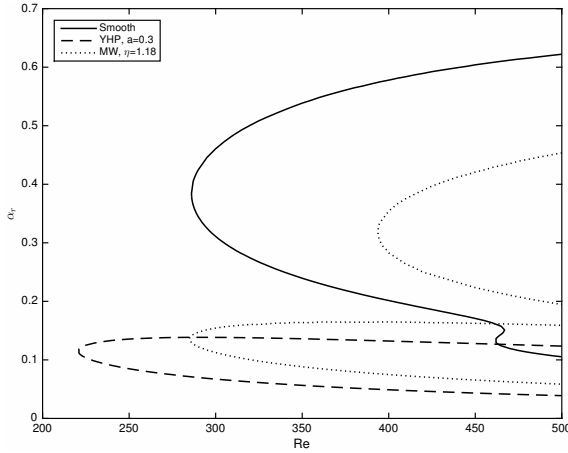
- (III) pressure work terms, obtained from $\{PW_i\}$,
- (IV) contributions from work done on the wall by viscous stresses, obtained from $\{S_i\}$,
- (V) terms arising from streamline curvature effects and the three-dimensionality of the mean flow, obtained from $\{G_i\}$.

Calculations have been carried out for both roughness models, and for both the Type I and II modes at $Re = 400$. The corresponding growth rates are shown in Figure 4. This emphasises the stabilising effect of roughness on the Type I mode, the destabilising effect on the Type II mode and the stronger effect on both of these modes for the YHP model. For the MW model the amplification of the Type II mode is more modest, even though the Type II lobe of the neutral curve shows similar augmentation to the YHP case, and the stabilising effect on the Type I mode is not quite so strong.

By calculating all terms in the energy equation (7) it is possible to identify where the effects of roughness are the greatest.



(a) Flow comparison



(b) Neutral curve comparison

Figure 3. Model comparison at $a = 0.3$ and $\eta = 1.18$.

Given the boundary conditions for the YHP model some terms in the energy equation are identically zero (PW_2, S_1, S_2, S_3). The results of the energy balance for the three roughness values $a = 0.1, 0.2$ and 0.3 are compared to those for a smooth disk ($a = 0$) in Figure 5. For both modes the main contributors are energy production by the Reynolds stress (P_2) and conventional viscous dissipation (D). Terms P_1, P_3, PW_1 and G_2 are found to be negligible and the geometric terms G_1 and G_3 remove energy from the system. The strongly stabilising effect of roughness on the Type I mode is manifested in a striking reduction in P_2 and a slight increase in viscous dissipation. Conversely, the growth with roughness of the Type II mode arises from a net increase in energy production through increased Reynolds stress alongside a reduction in viscous dissipation.

Results of the energy balance calculation for the MW model are shown in Figure 6. Again both modes are dominated by contributions from P_2 and D . The main difference from the YHP model in the case of the Type II mode is that, although the Reynolds stress energy production term increases as before, the MW model also shows an increase in viscous

YHP model			
	Re	n	ϵ
$a = 0$	286.1 (461.5)	22.2 (21.3)	11.4 (19.2)
$a = 0.1$	311.5 (394.4)	20.7 (16.7)	11.1 (19.5)
$a = 0.2$	426.8 (283.3)	20.6 (11.1)	10.8 (19.0)
$a = 0.3$	593.9 (220.6)	21.8 (8.5)	11.1 (18.5)
MW model			
	Re	n	ϵ
$\eta = 0$	286.1 (461.5)	22.2 (21.3)	11.4 (19.2)
$\eta = 0.14$	300.6 (390.3)	19.6 (17.5)	9.8 (16.9)
$\eta = 0.57$	343.7 (311.5)	15.4 (9.2)	7.3 (12.3)
$\eta = 1.18$	393.8 (284.9)	12.4 (6.3)	5.6 (9.2)

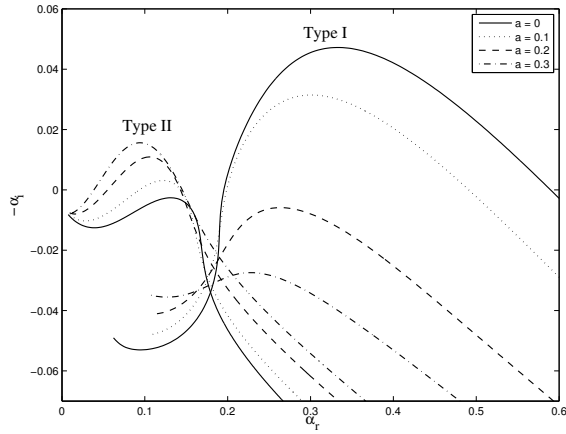
Table 1. Critical values of measurable parameters at the onset of instability under both models. Type I and (Type II). Bold text indicates the most dangerous mode in terms of critical Reynolds number.

dissipation (opposite to YHP) which would account for the more modest growth observed in Figure 4. The Type I mode shows a less pronounced decrease in P_2 , but more viscous dissipation compared to the YHP model.

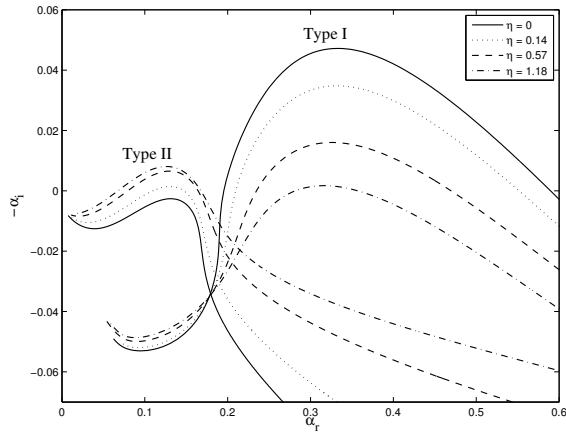
As detailed in publication [10] where a presentation of the disturbance eigenmodes is given, the Type II disturbances generally extend further into the boundary layer than the Type I disturbances. The further stretching of the disturbance profile of the YHP model as roughness is increased, together with the thickening of the boundary layer with roughness, would appear to contribute to the augmentation of the Type II instability mode. The MW model results in a similar stretching of the Type II eigenmodes to the YHP case. However, since there is no significant increase in the boundary-layer thickness for the MW steady flow, the fluid disturbances do not extend quite as far into boundary layer as for the YHP case. These affects appear to be related to the subtly different responses of the energy balance of the Type II mode across each roughness model. The Type I disturbance profiles are very similar to those for the YHP model.

5. CONCLUSION

We have summarised our theoretical study investigating the effects of radial anisotropic surface roughness resulting from concentric grooves on the stability of the von Kármán boundary-layer flow over a rotating disk. Our theoretical analysis was based on the two alternative approaches suggested by Yoon *et al.* [7] and by Miklavčič & Wang [8] for modelling the steady boundary-layer flow over a rough rotating disk. Our results have shown that both these fundamentally different approaches yield qualitatively consistent results for the two dominant steady-flow velocity components (radial and azimuthal) of the rotating-disk boundary layer for increasing roughness levels. Similarly, the subsequent linear stability analysis based on the steady-flow profiles obtained from the two modelling approaches revealed that in both cases the type



(a) YHP model



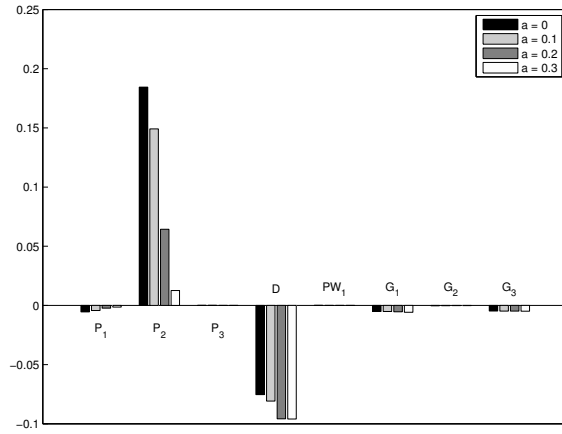
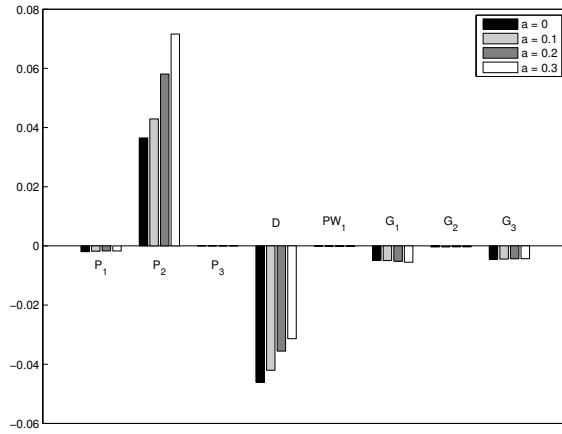
(b) MW model

Figure 4. Type I and II growth rate curves at $Re = 400$.

of roughness investigated results in a stabilisation of the Type I instability mode of the rotating-disk boundary layer and in a destabilisation of the Type II mode. However, it was found that, overall, the effects arising when following the YHP model are somewhat more pronounced than when using the MW approach.

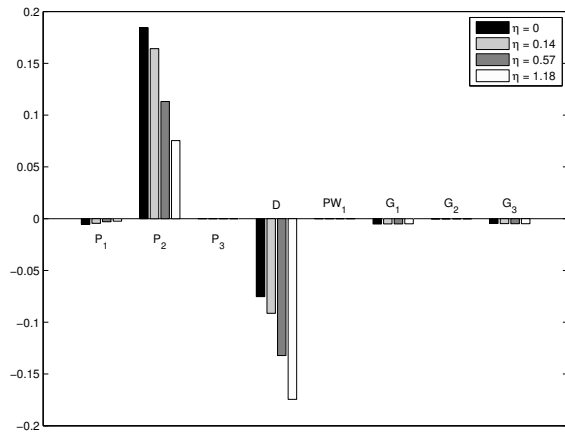
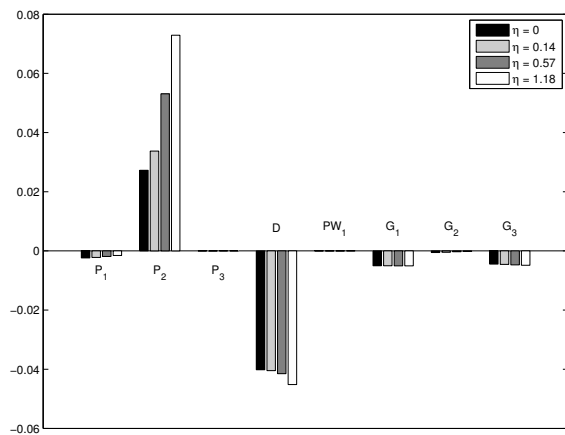
The energy analysis has revealed that for both the YHP and the MW approach, and for both the Type I and Type II instability modes, the main contributors to the energy balance are the energy production by the Reynolds stresses and conventional viscous dissipation. For the Type I mode dissipation increases with the roughness level and the increase is more pronounced for the MW model than for the YHP model. For the Type I mode Reynolds-stress energy production decreases with the roughness level and the decrease is more pronounced for the YHP model than for the MW model. Thus, in summary, increased energy dissipation and decreased energy production by Reynolds stresses implies a stabilisation of the Type I mode by increasing roughness levels.

For the Type II mode Reynolds-stress energy production increases with the roughness level and the increase is slightly less pronounced for the YHP model than for the MW model.

(a) Type I mode with $n = 28$.(b) Type II mode with $n = 12$.**Figure 5.** Results of energy analysis for YHP model at $Re = 400$.

The main qualitative difference is observed for the energy dissipation of the Type II mode. For the Type II mode energy dissipation decreases with the roughness level for the YHP model whereas there is a slight increase under the MW model. Yet, the overall increased Reynolds-stress energy production and decreased energy dissipation result in a destabilisation of the Type II mode for both the YHP and the MW model.

Our study suggests that the beneficial stabilisation of the Type I mode by concentric roughnesses becomes suppressed when the Type II mode is destabilised as it moves upstream and eventually becomes the critical mode at the lowest Reynolds number. This is consistent with our previous result [9]. The results of the energy analysis imply that the dissipation of the Type II mode is sensitive to the precise form of the steady-flow base profile. Consequently, maximising dissipation by an appropriately designed surface-roughness pattern, that leads to the energetically optimal base profile, can theoretically lead to an overall beneficial stabilisation of the Type II mode. Provided that the Type I mode is not adversely affected, this could result in a boundary-layer-transition delay and drag reduction. This points to a possible

(a) Type I mode with $n = 28$.(b) Type II mode with $n = 8$.**Figure 6.** Results of energy analysis for MW model at $Re = 400$.

way forward for exploiting the beneficial stabilising effects of radial anisotropic roughness on the Type I mode in future drag reduction techniques relying on transition delay for boundary layers with a cross-flow component.

Full details of this study into radial anisotropic roughness can be found in publication [10].

ACKNOWLEDGMENTS

SJG is supported by a Senior Research Fellowship of the Royal Academy of Engineering, funded by the Leverhulme Trust. SJG also wishes to acknowledge the hospitality of the Faculty of Science, School of Mathematics at the University of Sydney, Australia where the final version of this paper was completed. MÖ wishes to acknowledge financial support from Republic of Turkey Ministry of National Education.

REFERENCES

[1] Kármán, von Th. 1921 Ueber laminare und turbulente Reibung, *Z. Angew. Math. Mech.* **1**, 233-252.

[2] Lingwood, R.J. & Alfredsson, P.H. 2015 Instabilities of the von Kármán boundary layer, *Appl. Mech. Rev.* **67**, 030803.

[3] Saric, W.S., Reed, H.L. & White, E.W. 2003 Stability and transition of three-dimensional boundary layers, *Annu. Rev. Fluid Mech.*, **35**, 413-440.

[4] Sirovich, L. & Karlsson, S. 1997 Turbulent drag reduction by passive mechanisms, *Nature* **388**, 753-755.

[5] Carpenter, P. W. 1997 The right sort of roughness, *Nature* **388**, 713-714.

[6] Choi, K. S. 2006 The rough with the smooth, *Nature* **440**, 754.

[7] Yoon, M.S., Hyun, J.M. & Park, J.S. 2007 Flow and heat transfer over a rotating disk with surface roughness. *International Journal of Heat and Fluid Flow*, **28(2)**, 262-267.

[8] Miklavčič, M. & Wang, C.Y. 2004. The flow due to a rough rotating disk. *Z. angew. Math. Phys.*, **54**, 235-246.

[9] Cooper, A.J., Harris, J.H., Garrett, S.J., Thomas, P.J. & Özkan, M. 2015 The effect of anisotropic and isotropic roughness on the convective stability of the rotating disk boundary layer, *Phys. Fluids*, **27**, 014107.

[10] Garrett, S.J., Cooper, A.J., Harris, J.H., Özkan, M., Segalini, A. & Thomas, P.J. 2015 On the stability of von Kármán rotating-disk boundary layers with radial anisotropic surface roughness, to appear in *Phys. Fluids*.

[11] Malik, M. R. 1986 The neutral curve for stationary disturbances in rotating-disk flow. *J. Fluid Mech.* **164**, 275–287.

[12] Lingwood, R.J. 1995 Absolute instability of the boundary layer on a rotating disk, *J. Fluid Mech.* **299**, 17.

[13] Banks, W. H. H. 1965 The boundary layer on a rotating sphere. *Q. J. Mech. Appl. Math* **18**, 443–454

[14] Garrett, S.J. & Peake, N. 2002 The stability and transition of the boundary layer on a rotating sphere, *J. Fluid Mech.* **456**, 199-218.

[15] Lingwood, R.J. & Garrett, S.J. 2011 The effects of surface mass flux on the instability of the BEK system of rotating boundary layer flows, *European J. Mech. B* **30**, 299–310.

[16] Cooper, A.J. & Carpenter, P.W. 1997 The stability of rotating-disc boundary-layer flow over a compliant wall. Part 1. Type I and II instabilities, *J. Fluid Mech.* **350**, 231-259.

[17] Appelquist, E. 2014 Direct numerical simulations of the rotating-disk boundary-layer flow. Licentiate thesis, Royal Institute of Technology, KTH Mechanics, ISBN: 978-91-7595-202-4

- [18] Turkilmazoglu, M. & Gajjar, J.S.B. 1998 Convective and absolute instability in the incompressible boundary layer on a rotating-disk. Technical report, Department of Mathematics, University of Manchester.
- [19] Garrett, S.J., Hussain, Z. & Stephen, S.O. 2009 The cross-flow instability of the boundary layer on a rotating cone, *J. Fluid Mech.* **622**, 209-232.